J. Dairy Sci. 105:1940–1958
https://doi.org/10.3168/jds.2021-20538

Synthesis and physicochemical characterization of zinc-lactoferrin complexes

Oleksandra Pryshchepa,[1,2] Gulyaim Sagandykova,[1] Joanna Rudnicka,[1,2] Paweł Pomastowski,[1] Myroslav Sprynskyy,[2] and Bogusław Buszewski[1,2]*
[1]Centre for Modern Interdisciplinary Technologies, Nicolaus Copernicus University in Toruń, Wileńska 4, 87-100 Toruń, Poland
[2]Department of Environmental Chemistry and Bioanalytics, Faculty of Chemistry, Nicolaus Copernicus University in Toruń, Gagarina 7, 87-100 Toruń, Poland

ABSTRACT

One trend of the modern world is the search for new biologically active substances based on renewable resources. Milk proteins can be a solution for such purposes as they have been known for a long time as compounds that can be used for the manufacturing of multiple food and non-food products. Thus, the goal of the work was to investigate the parameters of Zn-bovine lactoferrin (bLTF) interactions, which enables the synthesis of Zn-rich protein complexes. Zinc-bLTF complexes can be used as food additives or wound-healing agents. Methodology of the study included bLTF characterization by sodium dodecyl sulfate-PAGE, MALDI-TOF, and MALDI-TOF/TOF mass spectrometry as well Zn-bLTF interactions by attenuated total reflection-Fourier-transform infrared, Raman spectroscopy, scanning and transmission microscopy, and zeta potential measurements. The obtained results revealed that the factors that affect Zn-bLTF interactions most significantly were found to be pH and ionic strength of the solution and, in particular, the concentration of Zn^{2+}. These findings imply that these factors should be considered when aiming at the synthesis of Zn-bLTF metallocomplexes.
Key words: bovine lactoferrin, zinc-lactoferrin interactions, whey proteins, metallocomplexes

INTRODUCTION

The connection between the quality of food and health has led to development of "functional foods," which implies the search and modification of naturally occurring compounds. Dairy products and their derivates are considered healthy and safe to consume, thus making them an attractive source for manufacturing new value-added goods (Ortiz et al., 2017). Proteins are the most valuable components of dairy products, and thus the production of food additives and supplements based on milk proteins is of high interest among dietitians, scientists, and food producers. Additionally, the utilization of milk proteins for the production of antibacterial agents is considered (Pomastowski et al., 2016; Buszewski et al., 2021).

Lactoferrin (**LTF**) is one of the most attractive milk proteins. Lactoferrin is a multifunctional protein belonging to the family of transferrins, which are non-heme iron-binding glycoproteins (Takayama, 2012). The transferrin family in mammals comprises serum transferrin (**TR**), LTF, and melanotransferrin (Baker, 1994). The main functions of both TR and LTF are Fe^{3+} transport and regulation. However, a more important function of the LTF is the host immune response for infection or inflammation (Lambert, 2012). The wide spectrum of biological activity of LTF also includes antimicrobial (Yoshida et al., 2000), antiviral (Waarts et al., 2005), antifungal (Andersson et al., 2000), immunoregulatory, and antiinflammatory properties (Grigorieva et al., 2019). Additionally, LTF plays a role in cell proliferation and migration; among others, topical administration of bLTF enhances wound closure (Takayama, 2012). What is interesting is that intravenously injected bovine lactoferrin (**bLTF**) was shown to be able to cross the blood-brain barrier (Takayama, 2012). Studies on adult mice have shown that bLTF given orally can absorb effectively from the intestine in an unchanged state (Fischer et al., 2007). Thus, the unique properties of LTF are the reason for the extensive investigations into LTF as a potential active drug substance (Wang, 2016; Sabra and Agwa, 2020). Lactoferrin can be used in pharmaceutical preparations with a wide spectrum of therapeutic effects: promotion of microelements absorption, boosting of the immune system, improvement of wound healing, including infected wounds, and so on. Indeed, preparations containing bLTF have already been developed. However, they usually are in the form of a mechanical

Received March 29, 2021.
Accepted October 18, 2021.
*Corresponding author: bbusz@umk.pl

mixture of zinc salts and LTF, which may not be as effective as Zn-protein complexes.

Zinc is an indispensable microelement that ensures numerous functions of an organism: protein structural component (zinc fingers and related motifs), co-factor of enzymes, signaling mediator, and so on (Kambe et al., 2015; Santos et al., 2020). Zinc deficiency is an issue in both developing and developed countries and is a subject of numerous research (Santos et al., 2020). The bioavailability of microelements is highly dependent on the form in which they are provided to the organism (Kawakami et al., 1993; Ianni et al., 2019). Increased bioavailability is observed for microelements in form of proteinates (Tang and Skibsted, 2016; Ianni et al., 2019). For instance, the Zn^{2+} and Fe^{2+} complexation with whey proteins significantly increased their uptake by Caco-2 cells as compared with inorganic salts (Shilpashree et al., 2020). Moreover, Zn^{2+} ions exhibit antibacterial properties (Bong et al., 2010; McDevitt et al., 2011), and in combination with bLTF may have a synergistic effect against a wide spectrum of microorganisms. Thus, such Zn-bLTF complexes may also have potential in wound healing preparations and can be a solution in the search for value-added goods derived from milk.

The metal-binding function of the transferrins is determined by their structure (i.e., by the presence of 2 intramolecular iron-binding sites comprising 2 tyrosines, aspartic acid, and histidine; Mizutani et al., 2012; Takayama, 2012). Apart from iron, the transferrins can reversibly bind other metals, and thus are suggested to play role in the metabolism of other metals, such as aluminum, manganese, copper, and zinc (Baker, 1994). Interestingly, Ainscough et al. (1980) reported that in human milk LTF appears with loosely bonded zinc, where zinc to protein ratio has the same order as iron to protein ratio. This may indicate the similar significance of LTF for zinc absorption as for iron. It is noteworthy to mention that the meaning of "saturated" regarding metalloproteins most often implies only the state when structurally defined metal-binding sites are filled. However, it was revealed that depending on conditions LTF can bind much more Fe^{3+} than can be explained only by the presence of intramolecular binding sites (Kawakami et al., 1993). For Zn^{2+}, it was shown that at least 2 additional metal-binding sites can appear at pH 8.6 on the surface of the C-lobe separated from LTF (Jabeen et al., 2005).

The process of metal ions binding to proteins is studied intensively as it is important and required for the understanding of the mechanisms of protein activity (e.g., catalytic), structural stability, and functional regulations (Gurd and Wilcox, 1956; Bou-Abdallah and Giffune, 2016). However, such studies mostly include only the process of the metals embedding into intramolecular binding sites. Nevertheless, the data indicate that zinc binding sites in proteins often include different combinations of histidines and cysteines. Moreover, glutamic and aspartic acid also can be involved in the chelation of the Zn^{2+} in proteins (Auld, 2013). What is interesting is that one of the action mechanisms of zinc in enzymes is the "water activation" by lowering its dissociation constant pK. Thus, zinc, while binding to protein, still can have water molecules in its coordination sphere (Auld, 2013; Bou-Abdallah and Giffune, 2016). Little information was found in the literature about the interaction of zinc with proteins through functional groups oriented to the surface of the protein. According to the existing knowledge, regardless of other conditions, stable Zn^{2+} complexes with proteins require the involvement of nitrogen-containing groups for metal chelation (Gurd and Wilcox, 1956; Yamauchi et al., 2002; Bou-Abdallah and Giffune, 2016; Alhazmi, 2019). Interestingly, the ability of Zn^{2+} to lower the pK of coordinated water molecules can lead to its dissociation and formation of ZnO. Such a feature of zinc was the reason for the formation of ZnO-protein nanocomposites, which were synthesized with the utilization of whey proteins (Shi et al., 2008) and ovalbumin (Buszewski et al., 2021). However, it should be noted that nanocomposites generally have a wider spectrum of toxic effects than other forms of metal compounds. The formation of homogeneous Zn-protein complexes was observed with the utilization of β-LG (Buszewski et al., 2020) and caseins (Pomastowski et al., 2014). The abovementioned facts indicate the need for the comprehensive study of the Zn-protein complexes formation.

Hence, the study aimed to investigate the parameters of Zn-bLTF interactions that enable the synthesis of homogeneous Zn-rich complex. One of the basic assumptions taken into account during the study was the formation of the Zn-bLTF complexes at any of the investigated conditions. The present study can be considered as an indispensable first step for the investigation of Zn-bLTF complexes as possible food additives for managing zinc deficiency or agents that promote wound healing, including infected wounds.

MATERIALS AND METHODS

Chemicals and Materials

The chemicals and materials used were of the highest available purity offered by suppliers. Standard lactoferrin from bovine milk (bLTF), ultrapure water

(liquid chromatography-MS purity >99%), acetonitrile, trifluoroacetic acid, ammonium bicarbonate, sodium bicarbonate, ammonium citrate dibasic, tri-sodium citrate dihydrate, sinapinic acid (**SA**), sodium chloride, sodium hydroxide, nitric acid, zinc nitrate hexahydrate, hydrochloric acid, dithiothreitol, iodoacetamide, Amicon Ultra Centrifugal membrane filters, ICP multielement standard solution IV, Zinc standard solution for ICP, and Scandium standard solution for ICP were purchased from Sigma-Aldrich. Invitrogen Bolt 4–12% Bis-Tris Plus polyacrylamide gel 10 and 12 wells, Simply Blue Safe Stain (Coomassie G_{250} stain), SeeBlue Plus 2 Pre-Stained Protein Standard, MES running buffer, load sample buffer, and sample reducing agent were supplied by ThermoFisher Scientific. Peptide calibration standard II, protein calibration standard II, α-cyano-4-hydroxycinnamic acid (**HCCA**), AnchorChip, and GroundSteel target plates were obtained from Bruker Daltonics. A set of automatic pipettes and all laboratory plastics were obtained from Eppendorf. Moreover, trypsin for protein MS from Promega was used. Deionized water was obtained with the Milli-Q RG system from Millipore (Millipore Intertech).

Characterization of LTF

Zeta Potential Measurements and Isoelectric Point Determination. Zeta (ζ) potential measurements were performed on a Malvern Zetasizer NanoZS (Malvern) using a DTS1070 cuvette (Malvern). The analysis was carried out in the automatic selection mode of voltage and number of runs. The results were obtained taking into account the Smoluchowski approximation (Oćwieja et al., 2015):

$$\zeta = \eta\mu_e/\varepsilon_r\varepsilon_0\,, \qquad [1]$$

where η = solution viscosity; μ_e = electrophoretic mobility; ε_0 = electric permeability in vacuum, and ε_r = dielectric constant of the solution.

Each measurement was performed in triplicate. For isoelectric point (**pI**) determination, the zeta potential was measured as a function of pH. The potentiometric acid-base titration in the pH range from 4.0 to 9.0 was performed with the utilization of 1 mg/mL of bLTF solution obtained by protein suspension in 0.09% NaCl. The pH adjustment was performed by a dropwise addition of 0.1 *M* hydrochloric acid or 0.1 *M* sodium hydroxide solutions. Here and later, the pH of the solutions was determined using the FiveEasy Plus pH meter (Mettler Toledo) with a combined electrode with glass membrane and Ag/AgCl reference system (Mettler Toledo). Before the measurements, the pH meter was calibrated by standard buffered solutions with pH values 4.0, 7.0, and 10.0.

Intact Protein Analysis by MALDI-TOF-MS. Sinapinic acid was used as a matrix for MALDI analysis. Intact protein was suspended in the 0.1% trifluoroacetic acid to a concentration of 10 mg/mL. The saturated solution of SA was prepared in the TA30 solvent [30:70 (vol/vol) acetonitrile:0.1% trifluoroacetic acid]. Then, 1 μL of the samples was applied on the GroundSteel target plate by dried droplet technique with utilization of 1 μL of the matrix solution. Protein calibration standard II was used for mass calibration. All the MS spectra were obtained using the MALDI-TOF/TOF mass spectrometer UltrafleXtreme (Bruker Daltonics) equipped with modified neodymium-doped yttrium aluminum garnet (Nd:YAG) laser operating at a wavelength of 355 nm and frequency of 2 kHz. The system was controlled using the Bruker Daltonics software (flexControl and flexAnalysis). The MS spectra were obtained in the linear positive mode in an m/z range of 10,000 to 100,000, applying an acceleration voltage of 25 kV and the minimum laser power of 60% and attenuation of 50%. Spectra were acquired by summing up 3 individual spectra obtained with 500 laser shots each and were plotted using the Origin software (v. 2015, OriginLab Corp.) from raw data without any modifications.

SDS-PAGE Coupled to Protein In-Gel Tryptic Digestion and MALDI-TOF/TOF-MS Analysis. The SDS-PAGE separation was carried out by the standard procedure recommended by the manufacturer. In-gel tryptic digestion was carried out by procedure described in the study by Shevchenko et al. (2006) with only one modification [i.e., the digestion step was performed by the protocol recommended by the producer of trypsin (Promega)]. For MALDI-TOF/TOF-MS analysis, the HCCA was used as a matrix. The matrix solution was prepared as follows: HCCA was dissolved in a mixture containing 85% acetonitrile, 15% ultrapure water, and 0.1% trifluoroacetic acid to a final concentration of 1.4 mg/mL. One microliter of the protein tryptic digest solutions was applied on an AnchorChip target plate by dried droplet technique with the utilization of 1 μL of the matrix solution. Peptide calibration standard II (Bruker Daltonics) was used for mass calibration. The MS spectra for protein digests (peptide fingerprints mass spectra) were recorded in a reflectron positive mode in the range of m/z 500 to 3,500. The measurements were performed with the utilization of acceleration voltage of 25 kV, minimum laser power of 80%, and attenuation of 27%. Spectra were acquired by summing up 3 individual spectra obtained with 500 laser shots each. The peptide spectra analysis was carried out using the BioTools and ProteinScape software

(Bruker Daltonics). Protein identification was carried out by applying Mascot search with nonstandard search parameters (i.e., cysteine modified by carbamidomethylation) and mass tolerance was set to 0.1 Da.

Preparation of Samples for the Study of Zn-Lactoferrin Interactions

The Zn-bLTF interaction study was performed in 3 different buffers, namely 0.09% sodium chloride solution pH 6.0; 0.1 *M* ammonium bicarbonate/ammonium citrate buffer, pH 7.4; and 0.1 *M* sodium citrate/sodium, bicarbonate buffer, pH 8.6. Each of the buffers was prepared as follows: sodium chloride was dissolved in deionized water and adjusted to pH 6.0 with 0.1 *M* sodium hydroxide or 0.1 *M* hydrochloric acid; 0.1 *M* ammonium bicarbonate was prepared in deionized water and adjusted to pH 7.4 with 0.1 *M* ammonium citrate solution; and 0.1 *M* sodium bicarbonate and 0.1 *M* trisodium citrate were prepared in deionized water, mixed (1:1, vol/vol), and adjusted to pH 8.6 with 0.1 *M* sodium hydroxide solution. The bLTF was suspended in the buffers to gain the concentration of 5 mg/mL (by weight). The Zn^{2+} solutions were obtained from stock (6 g/L prepared from $ZnNO_3$ in deionized water) by dilution in the buffers to obtain solutions with a metal concentration of 6, 60, and 600 mg/L (the exact Zn^{2+} concentrations were measured by ICP-MS). The bLTF and Zn^{2+} solutions were mixed at the ratio 1:1 (vol/vol) and incubated with stirring for 24 h at room temperature (≈23°C). The protein after interaction with Zn^{2+} (product of interaction) was separated and washed twice with ultrapure water to remove the electrolytes excess by utilization of membrane filters cut-off 3 kDa (Amicon Ultra Centrifugal Filters). The obtained products were lyophilized and subjected to analysis. Moreover, the obtained first supernatant was analyzed for the determination of the Zn^{2+} adsorption capacity of protein.

Characterization of Prepared Samples

ICP-MS Analysis. Metal quantification in the solutions was performed on a Shimadzu ICP-MS 2030 with scandium as an internal standard. Determination of the metal content in bLTF and the products of Zn-bLTF interactions were carried out on mineralized samples. Nearly 2 mg of the samples was placed in Eppendorf tubes and mixed with 100 μL of nitric acid. Then, the Eppendorf tubes were closed tightly and heated at 80°C for 3 h. The mineralized samples were quantitatively transferred to polypropylene tubes and diluted with ultrapure water. Subsequent dilutions were performed with 1% HNO_3. The obtained solutions were subjected to inductively coupled plasma (**ICP**)-MS analysis.

For the determination of the metal adsorption capacity of protein, the equilibrium concentration of Zn^{2+} in the supernatant was determined. The supernatant dilutions were performed with 1% HNO_3 in polypropylene tubes. The adsorption capacity was calculated according to

$$q = \frac{(C_0 - C) \times V}{m}, \quad [2]$$

where q is the amount of adsorbed Zn^{2+}, m is the mass of the protein dispersed in the reaction mixture (g), C_0 is the initial concentration of Zn^{2+} in the reaction mixture (mg/L), C is the equilibrium concentration of Zn^{2+} in the reaction mixture (mg/L), and V is the volume of the reaction mixture (L).

Fourier Transform Infrared Spectroscopy. Fourier transform infrared spectroscopy (**FTIR**) analysis was performed for verification of the changes as a result of bLTF interactions with Zn^{2+}. Infrared spectra for both native bLTF and after incubation with Zn^{2+} in different conditions were recorded in the mid-infrared range (4,000–400 cm^{-1}). The spectra were collected with the utilization of attenuated total reflection (**ATR**) mode on Alpha FTIR spectrometer (Bruker). The FTIR spectra were plotted using the Origin software (v. 2015, OriginLab Corp.).

Raman Spectroscopy. Raman spectroscopy as a complementary technique for FTIR was performed to distinguish more precisely the functional groups that may be involved in the interactions between bLTF and Zn^{2+}. The bLTF and the products of Zn-bLTF interactions were placed on borosilicate microscope slides. The Raman spectra were recorded on Senterra II Dispersive Raman Microscope (Bruker) in the range of 4,000 to 400 cm^{-1}. The excitation wavelength at $\lambda = 532$ nm was used with a power of 20 mW. Raman spectra were plotted using the Origin software (v. 2015, OriginLab Corp.) and were normalized by a signal of the amide I band.

Electron Microscopy. The products of Zn-bLTF interaction dispersed in ethanol were placed on a carbon-coated copper grid (Lacey Carbon Support Film 400 mesh, Electron Microscopy Sciences), dried at room temperature, and subjected to analysis by transmission electron microscopy coupled with an energy-dispersive X-ray spectrometer (TEM-EDX-FEI Tecnai F20 X-Twin) and scanning electron microscopy (LEO 1430 VP, LEO Electron Microscopy Ltd.).

RESULTS AND DISCUSSION

Interactions Between BLTF and Zinc

The bLTF was analyzed using gel electrophoresis with a 4 to 12% gradient. Numerous bands of proteins were observed in the range of 14 to 198 kDa (Figure 1). The obtained results indicated the presence of multiple impurities in the product as well as bLTF dimer. The supplier declared the purity of the standard to be not less than 85% by SDS-PAGE assay. This emphasizes the need to perform characterization of the target protein before the study of the interactions with metal ions. The presence of other proteins in the sample may affect the binding of the studied metal ions to the target protein. Interactions of the proteins from impurities can be assigned as interactions of the target protein with metal ions and lead to distorted interpretation of the results.

Ion-exchange chromatography is one of the most common techniques for the isolation and purification of bLTF (Ye et al., 2000; Yoshida et al., 2000). The high isoelectric point of bLTF (higher than 8; Takayama, 2012) enables its selective isolation from other whey proteins. Lactoperoxidase is another whey protein that has a pI value (9.2–9.9) and molecular weight close to bLTF (89 kDa), which makes it the major impurity of bLTF. However, the concentrations of lactoperoxidase in the bLTF isolates usually are at a very low level and can be neglected (Du et al., 2013). Another source of the bLTF impurities may arise from the degradation as a result of the cleavage of the protein chain during isolation or storage. Proteins can undergo multiple reactions that affect their biological activity; among others, peptide bond hydrolysis and protein oxidation may be a reason for their fragmentation. Peptide bond cleavage occurs in the presence of water and is promoted even under mildly acidic conditions (Simpson, 2010). Whey acidification is usually used for casein separation and is one of the major steps in whey protein fractionation (Yoshida et al., 2000; Pomastowski et al., 2016). Moreover, acidification as well as other technological processes such as spray-drying, high-pressure treatment, and so on can lead to partial protein denaturation and therefore to higher susceptibility to the protein primary structure degradation. It should be noted that metal

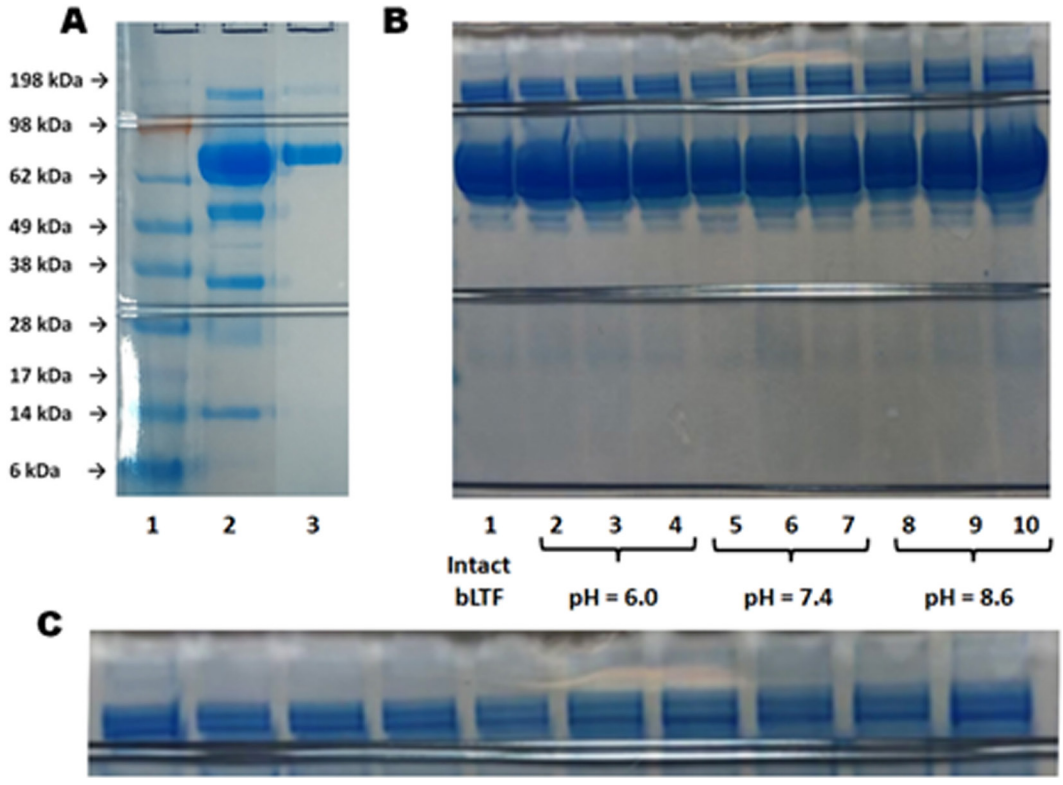

Figure 1. Sodium dodecyl sulfate-PAGE electropherogram of (A) protein markers (lane 1), intact bovine lactoferrin (bLTF; lane 2), and bLTF after membrane ultrafiltration (lane 3) with cut-off 50 kDa; (B) intact bLTF (lane 1); from left to right products of bLTF interaction with Zn^{2+} at pH 6.0, 7.4, and 8.6 with metal concentration of 6 mg/L (lanes 2, 5, and 8), 60 mg/L (lanes 3, 6, and 9), and 600 mg/L (lanes 4, 7, and 10), respectively; and (C) enlarged fragment of the electropherogram B corresponding to dimer bands.

ions are important factors that stabilize the proteins against degradation by tertiary structure stabilization (Kambe et al., 2015; Franco et al., 2018). Considering the bLTF structure, the peptide bridge connecting the 2 protein lobes is the most compliant place for degradation and enzymatic digestion (Takayama, 2012). The SDS-PAGE analysis showed the band between 38 and 49 kDa, which can correspond to the parts of bLTF molecule such as the N-lobe and C-lobe. The smaller proteins, with bands present on the electropherogram, can be derivatives of bLTF further cleavage. From Figure 1A, it can be observed that it was possible to obtain the pure bLTF by membrane ultrafiltration with a 50 kDa cut-off value. Thus, it can be suggested that all impurities were introduced during the LTF isolation and storage. Moreover, bLTF ordered from another lot revealed almost no evidence of impurities (Figure 1B.1).

The SDS-PAGE analysis of the protein after interaction with Zn^{2+} did not show significant changes in the intensity and position of the main band of bLTF. However, slight changes in the electrophoretic mobility of the bLTF dimer band can be observed (Figure 1C). The changes in the protein mobility were observed for all samples obtained at pH 8.6 and pH 7.4, where the highest changes were for samples synthesized at pH 8.6 and with the utilization of higher Zn^{2+} concentration. In the previous study of bLTF by PAGE-IEF, such slight changes in electrophoretic mobility were observed for the protein with different iron saturation levels, which influences the pI value (Voswinkel et al., 2016). Thus, it can be deduced that changes in the electrophoretic mobility may be due to the Zn^{2+} binding to the protein. However, it should be noted that such drift of the protein band position can also be due to interference of the excess of ions in the sample, which comes from the buffer used. Still, it was shown that NaCl up to a concentration of 0.4 *M* has little effect on the migration of the protein bands (See et al., 1985). In the study, the buffers used had a concentration of 0.1 *M* and the samples were washed twice with ultrapure water after synthesis.

By utilization of MALDI-TOF-MS in linear positive mode, it was possible to estimate the molecular weight of bLTF ($[M+H]^+$) (Figure 2). Average masses of bLTF were in the range of 82 to 84 kDa with a maximum of nearly 83,200 Da. In the previous study of our group, the average masses of isolated bLTF were in the range of 77 to 81 kDa with a maximum of 77,700 Da (Pomastowski et al., 2016). Bovine lactoferrin is the glycoprotein and the differences in masses are related to its glycosylation degree. Bovine lactoferrin has 5 possible glycosylation sites and 4 of them are always glycosylated (Asn233, 368, 476, and 545), whereas the fifth (Asn281) is glycosylated in about 15 to 30% depending on the stage of lactation (van Veen et al., 2004). Moreover, the level of bLTF glycosylation is also dependent on other factors such as inflammation, environmental, and stress conditions (Wei et al., 2000). Yoshida et al. revealed that 2 different forms such as bLTF-a (molecular mass, M_r, $\approx$ 84,000) and bLTF-b ($M_r \approx$ 80,000) can be isolated both from colostrum and mature milk (Yoshida and Ye-Xiuyun, 1991; Yoshida et al., 2000). Moreover, it was shown that bLTF-a is more resistant to proteolytic degradation than bLTF-b. Additionally, a previous study has shown that bLTF-a displays a higher bacteriostatic activity against *Escherichia coli* than bLTF-b (Yoshida et al., 2000). The studies indicated the significance of the degree of glycosylation of proteins on their biological activity, which should be taken into account during the investigation. Other signals were suggested to correspond to multiple-charged bLTF ($[M+2H]^{2+}$) ions and the impurities in the sample, namely $[M_1+H]^+$, signals marked by F, and other smaller proteins. On the spectrum of the protein after filtration with 50 kDa cut-off, only the signals from multiple-charged ions of bLTF can be seen and additional small signals of some impurity near 22.5 ($[M_2+H]^+$) and 14 kDa. Still, it should be noted that even though protein degradation is an unwanted process, the peptides derived from whey proteins have numerous useful properties. For instance, lactoferricin of bLTF reveals even higher bactericidal ability than bLTF itself (Takayama, 2012; Dullius et al., 2018).

Further bLTF samples were subjected to SDS-PAGE separation and in-gel tryptic digestion coupled to MALDI-TOF/TOF-MS analysis, which enabled the identification of 6 proteins that were found to be the most abundant in the mixture. Almost all studied proteins were identified as bLTF as well as its dimer and fragments, but the protein with a mass of nearly 14 kDa was shown to be bovine keratin. The obtained results may serve as additional evidence of the bLTF degradation during isolation and storage as the main source of impurities as was suggested from SDS-PAGE analysis (Figure 1). All subsequent analyses, including the studies of bLTF-Zn interactions, were performed using the bLTF standard with higher purity with no additional purification.

Zeta potential measurement is usually used for the characterization of electrochemical properties of biomolecules. The knowledge about proteins' net charge is important for the prediction of their behavior in the solutions (e.g., their dispersion stability, interaction with sorbents or membranes during separation and purification). One of the applications of ζ-potential measurements is the protein pI determination, at which

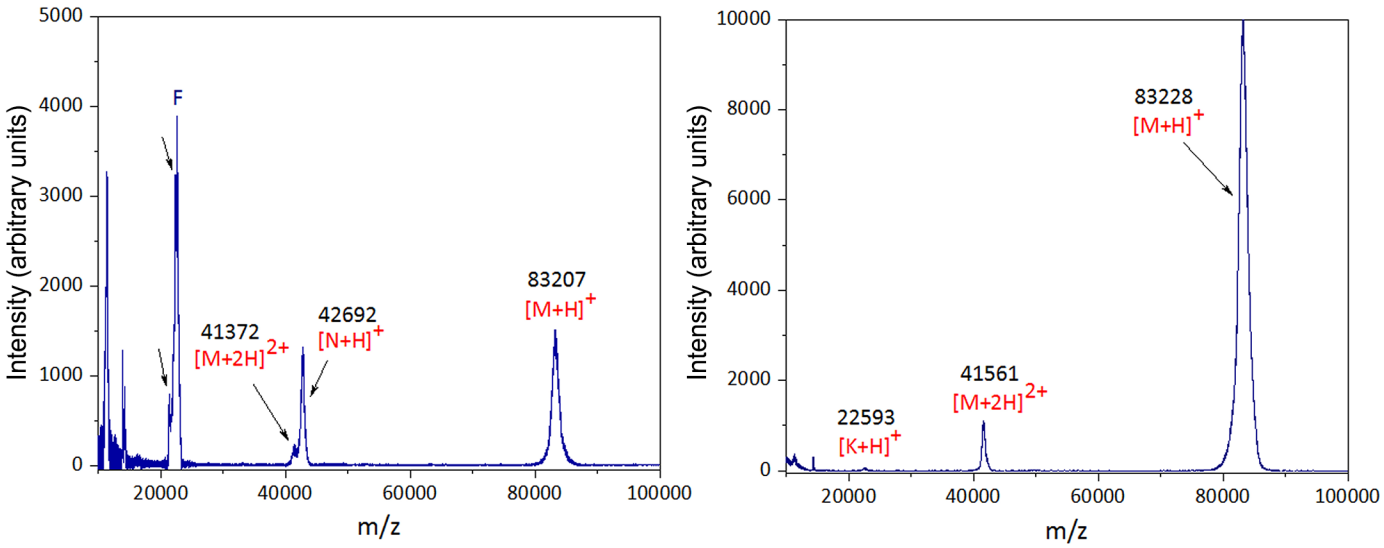

Figure 2. The MALDI-TOF-MS spectra of native bovine lactoferrin (bLTF; on the left) and bLTF after membrane filtration with cut-off value 50 kDa; signals $[M_1+H]^+$, $[M_2+H]^+$, and F correspond to signals of impurities.

the net charge of the protein equals zero. At pI proteins become more hydrophobic, compact, and less stable, and hence can easily aggregate and precipitate (Salgın et al., 2012). What is important is that the protein net charge may affect the process of metal-protein interaction (Gurd and Wilcox, 1956; Roosen-Runge et al., 2013). Thus, the pI value is an important parameter for the description of the mechanisms of metal binding to protein.

In our study, the protein acid-base potentiometric titration has shown that, as a function of pH (Figure 3), ζ-potential values of bLTF vary from +20 to −6 mV at the pH values of 4 to 9. The ζ-potential changes in the specified pH range fit a linear model. This allows determining the pI value of bLTF, which was established at pH = 7.4 ± 0.2. The utilization of other models did not show significant changes. The majority of literature sources indicate a bLTF pI value in a range between 8.0 and 9.0 (Lambert, 2012; Takayama, 2012). The differences in the pI values are related to differences in the measurement technique used. For instance, for A-type lipase of *Candida antarctica* pI value at 4 was determined by electrophoretic mobility, whereas the isoelectric focusing technique showed the pI value as 7.5 (Salgın et al., 2012). Moreover, the studies performed in our group have shown that depending on the ions present in the solution the determined pI values for β-LG were from 5.3 to 7.6 within the same technique (Gołębiowski et al., 2020). The study indicates the high importance of the effect of specific protein-ion interactions on the obtained results. Moreover, the ionic strength of the dispersion medium also can result in differences in pI values (Salgın et al., 2012). What is interesting is that the previous investigation performed in our group for bLTF with molecular weight ≈78 kDa has revealed a pI value of 6.0 ± 0.3 (Pomastowski et al., 2016). Both in the present study and in the one performed by Pomastowski et al. the conditions for pI determination of bLTF were the same, namely the protein was titrated in 0.09% NaCl, indicating the influence of the glycosylation level on the electrochemical features of proteins.

The spectra obtained within ATR-FTIR analysis of native bLTF have revealed a typical pattern of absorption bands (Figure 4). The bands that occurred in the region from 2,800 to 3,700 cm^{-1} represent stretching (str.) vibrations related to hydrogen-containing groups.

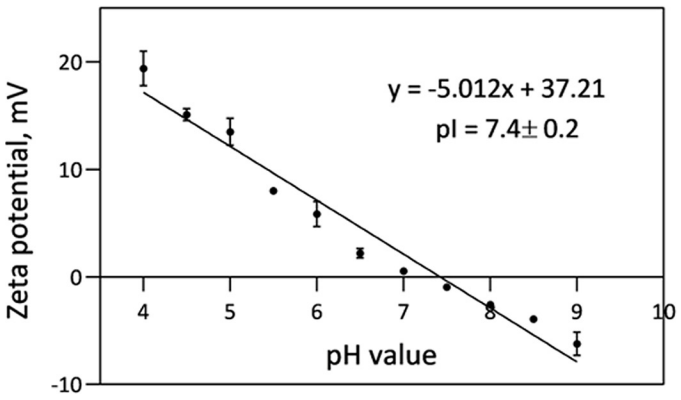

Figure 3. Zeta potential of bovine lactoferrin as a function of pH. pI = isoelectric point.

The absorption band with a maximum at 3,280 cm^{-1} corresponds to O–H and N–H str. vibrations. The broad shape of the band indicates the involvement of amino and hydroxyl groups in the hydrogen bond. The bands at 3,078, 2,980, 2,936, and 2,886 cm^{-1} come from C-H asymmetric and symmetric stretching vibrations of CH_3 and CH_2 groups as well as aromatic rings (Nandiyanto et al., 2019). Additional band for $\delta_{as}(CH_3)$ (1,472 cm^{-1}) is almost undetectable on the spectrum of native bLTF due to signals overlay. Instead, the band for $\delta(CH_2)$ was visible at 1,451 cm^{-1} (Barth, 2007; Nandiyanto et al., 2019). After interaction with Zn^{2+} in all of the samples, the new band at 3,653 cm^{-1} has appeared. The band might appear due to the unbounded O–H group vibrations, which are more often connected to the presence of water in the sample, but also may be due to the hydrogen bonds destruction in the protein (Socrates, 2004). The results may indicate that the samples were not dried completely after the synthesis. However, the signals were even more intense in samples obtained at pH values 7.4 and 8.6. As Zn^{2+} appears in the solution as aqua complex (Krężel and Maret, 2016), the results may indicate the metal adsorption on the protein surface with a coordination sphere partially filled with water molecules, thus enhancing the water signal in the spectrum. It should be noted, that water always accompanies the protein molecules. Some scientists claim that water molecules are the indispensable part of the protein that take part not only in the tertiary structure formation but also participate actively in the protein reactions, for instance in the directed proton transfer (Kotting and Gerwert, 2007). More interestingly, the unusual enhancement of the signals of the methyl and methylene groups was observed, especially in the samples formed at pH 7.4 and 8.6, which may be due to the changes in the protein crystal structure rearrangement. For instance, similar but less significant effects were observed in the case of the study of solid to liquid transitions in long-chain alkanes (Corsetti et al., 2017). In the fingerprint region, the signal 1,637 cm^{-1} was assigned to the characteristic band for the peptide bond of amide I. The absorbance of the band in ≈80% is due to CO str. vibrations (Socrates, 2004). However, the out-of-phase C-N str. vibration and NH in-plane bending (≈10% each) also contribute to the amide I band (Socrates, 2004; Barth, 2007). The position of the band is dependent on the protein secondary structure and indicates the presence of a large number of β-sheet structures in the bLTF molecule. The data derived from crystallography studies also indicate a high amount of β-sheet in the proteins from the transferrin family (Baker, 1994; Mizutani et al., 2012; Takayama, 2012). The amide II band, which comes from out-of-phase NH in-plane bending and the CN str. vibration with a small contribution from CO in-plane bending and CC/NC str. vibrations, was observed at 1,533 cm^{-1} (Socrates, 2004; Barth, 2007). The bands appeared at 1,338 cm^{-1}, 1,309 cm^{-1} (α-helix), and 1,240 cm^{-1} (β-sheet) can be assigned to amide III modes, which mainly comes from CN str. and NH bending (≈30% each; Singh et al., 1993; Barth, 2007). The more intense band at 1,240 cm^{-1} also indicates the prevalence of β-sheet structures in the protein molecule. The enhancement and shifts of the amide III bands after protein interaction with Zn^{2+} may indicate the metal complexation through NH and CN groups and changes in protein secondary structure (Socrates, 2004). The relatively strong absorption band at 1,391 cm^{-1} can be attributed to $\nu_s(COO^-)$ of glutamic and aspartic acids (Nandiyanto et al., 2019). The band may shift significantly upon cation chelation (+60/−90 cm^{-1}). Bovine lactoferrin has 40 glutamic and 36 aspartic acid residues in a single molecule, which makes up 11% of the total number of residues and may indicate the high potential in metal ion chelation (Pomastowski et al., 2016). The bands at 1,159 cm^{-1} and 1,129 cm^{-1} can be assigned to ν(C–O) of serine, aspartic, and glutamic acid, whereas the band at 1,067 cm^{-1} comes from ν(C–O) of threonine. The band that occurred at 967 cm^{-1} could also arise from the serine residue (Barth, 2007). The significant enhancement of the bands after protein interaction with Zn^{2+} indicates the changes in the composition of the accompanying metal ions in the protein and the involvement of all of the assigned AA, namely serine, aspartic, and glutamic acids. The bands below the 800 cm^{-1} come from amide IV–VII, the interpretation of which is hard to perform due to a lack of information for protein in the literature (Socrates, 2004). Detailed changes in FTIR bands and their intensities can be found in Table 1, where an increase or decrease in intensities was assigned by arrows.

Raman spectroscopy can be considered as complementary to FTIR vibrational spectroscopic technique, which can provide more structural details on chromophores as they are saturated in π-electrons and thus can be polarized more easily (Wen, 2007). Obtained Raman spectra of native bLTF have several absorption bands, characteristic for proteins (Figure 5). The broad band with a maximum at 3,325 cm^{-1} can be assigned to O–H and N–H str. vibrations involved in hydrogen bonding (Socrates, 2004). The band at 3,055 cm^{-1}could also be due to N–H str. vibrations, whereas intensive bands at 2,931 and 2,873 cm^{-1} come from aliphatic C–H str. vibrations. The band of amide I appeared at 1,669 cm^{-1}. Similar to FTIR, the position of the amide I band indicates the high impact of β-sheet structures

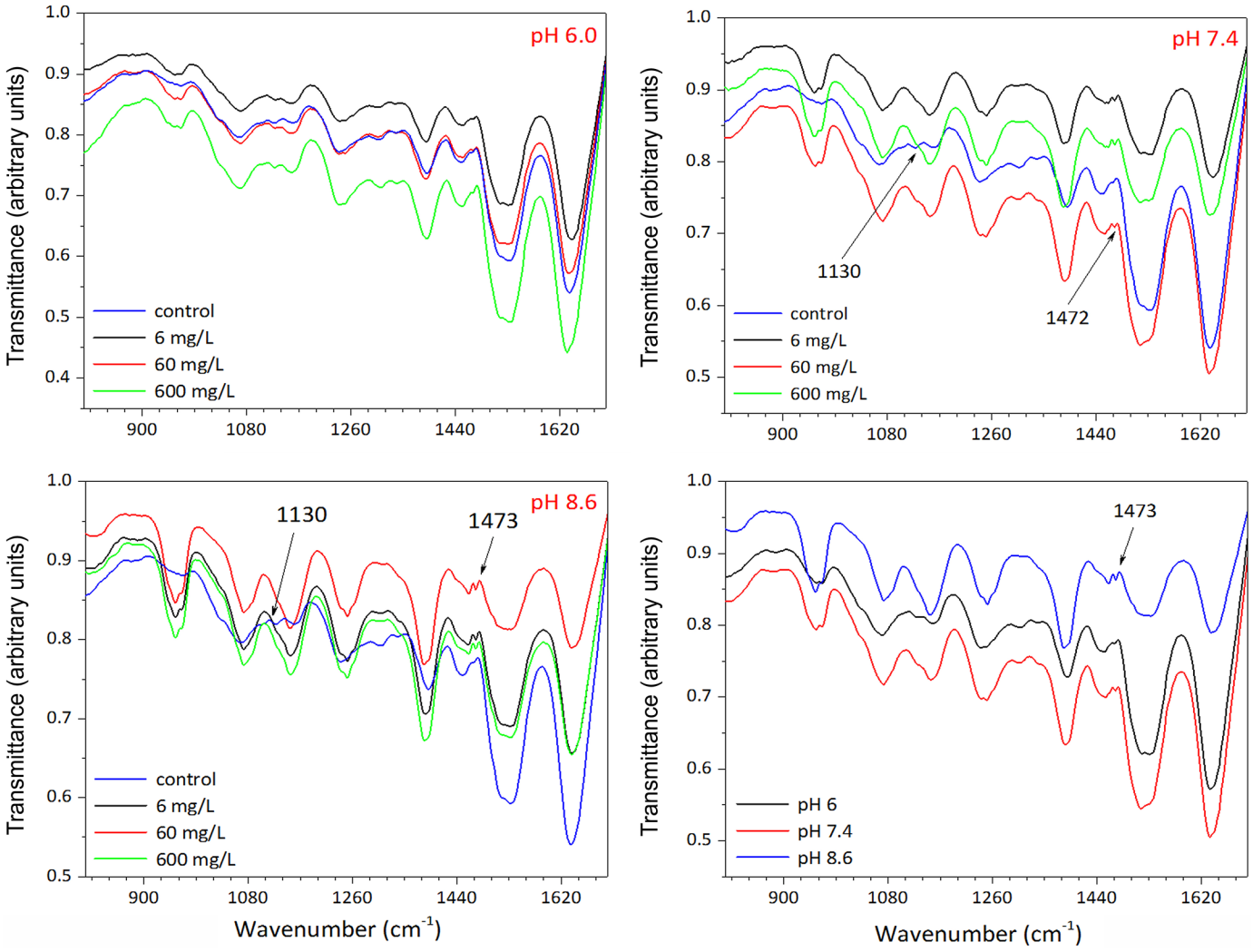

Figure 4. Attenuated total reflection-Fourier-transform infrared spectra of native bovine lactoferrin (bLTF) and bLTF after interactions with Zn^{2+} (fingerprint region).

in the molecule. However, in the amide III region, the intensive band at 1,284 cm^{-1} and the less intensive one at nearly 1,329 cm^{-1} should indicate the presence of all structures, namely α-helix, β-sheet, and random coils (Wen, 2007). The changes in the signal distribution of the amide III bands after bLTF interaction with Zn^{2+}, the same as in the FTIR spectra, may indicate the changes in the secondary structure of the protein as well as the significant role of CN and NH groups in metal ion binding. What is interesting is that according to literature data the amide II band should have low intensity in Raman spectra (Socrates, 2004; Jacob et al., 2009). However, in our study, the vibrational band at 1,503 cm^{-1}, which may be related to amide II, has rather medium intensity. The band at 1,602 cm^{-1} was assigned to ring modes of aromatic residues, namely phenylalanine, tyrosine, and tryptophan. The additional bands for each of the residues can be found at 1,206, 1,168, and 835 cm^{-1} for tyrosine, 1,035 and 1,003 cm^{-1} for phenylalanine as well as 1,550 (indole ring modes), and 874 and 757 cm^{-1} for tryptophan (Wen, 2007; Rygula et al., 2013).

What is important is that the bands of these AA are sensitive to the local environment. Moreover, the π-cation interactions affect some of the bands such as 757 and 1,550 cm^{-1} of tryptophan, which should be helpful for the study of metal-protein interactions (Wen, 2007). Thus, the changes in relative intensities of the bands indicate the changes in the cation content in the protein. The bands at 1,450 and 1,096 cm^{-1} correspond to C–H and C–N deformation vibrations (Rygula et al., 2013). The bands that occurred in region 500 to

Table 1. The assigned bands derived from attenuated total reflection-Fourier-transform infrared spectra of native bovine lactoferrin (bLTF) and after interaction with Zn^{2+1}

		Products of Zn-bLTF interaction								
		pH 6.0			pH 7.4			pH 8.6		
Assignment	Native bLTF	6 mg/L	60 mg/L	600 mg/L	6 mg/L	60 mg/L	600 mg/L	6 mg/L	60 mg/L	600 mg/L
Nonbonded O–H str., OH str. of water molecules	—	3,653↑	3,646↑	3,647↑	3,656↑↑	3,655↑↑	3,655↑↑	3,657↑↑	3,658↑↑	3,655↑↑
N-H str.; bonded O–H,	3,283	3,292	3,283	3,275	3,292	3,283	3,283	3,284	3,294	3,293
aliphatic and aromatic	3,078	3,079	3,078	3,082	3,076	3,068	3,068	3,086	3,079	3,078
C–H sym/asym. str.	2,970	2,980↑↑	2,980↑↑	2,980↑↑	2,980↑↑	2,980↑↑	2,980↑↑	2,980↑↑	2,980↑↑	2,980↑↑
	2,934	2,936	2,932↑	2,934↑	—	2,932↑	2,932↑	2,932↑	2,932↑↑	2,933↑↑
	2,876	2,886	2,885↑	2,885↑	2,888	2,889↑	2,889↑↑	2,888↑↑	2,888↑↑	2,889↑↑
Amide I band	1,637	1,642	1,636	1,633	1,643	1,635	1,636	1,639	1,638	1,638
Amide II	1,533	1,532	1,531	1,537	1,537	1,516	1,516	1,532	1,528	1,533
δas.(CH_3)	1,468	1,471	1,471↑	1,470	1,472↑	1,472↑	1,473↑	1,473↑	1,473↑	1,473↑
δ(CH_2)	1,451	1,454	1,454↑	1,453	1,456↑	1,455↑	1,456↑	1,460↑	1,460↑	1,460↑
Asp, Glu $\nu_s(COO^-)$	1,391	1,390↑	1,390↑	1,391↑	1,384↑↑	1,386↑↑	1,384↑↑	1,385↑↑	1,383↑↑	1,384↑↑
Amide III	1,338	1,337	1,338↑	1,339↑	—	—	—	—	—	—
	1,309	1,306	1,307↑	1,312↑	1,304	1,307	1,314	1,306	1,314	1,311
	1,240	1,250/1,241↑	1,250/1,240↑	1,249/1,241↑	1,241/1,251↑↑	1,241/1,250↑↑	1,251↑↑	1,251↑↑	1,251↑↑	1,251↑↑
Asp,Glu, ν(C–O)/Ser,	1,159	1,159↑	1,158↑	1,158↑	1,153↑↑	1,155↑↑	1,153↑↑	1,153↑↑	1,151↑↑	1,153↑↑
ν(CO), δ(CO_2H)	1,129	1,130↑	1,129↑	1,128↑	—	—	—	—	—	—
Thr ν(C–O)	1,067	1,071↑	1,070↑	1,071↑	1,072↑↑	1,072↑↑	1,071↑↑	1,072↑↑	1,072↑↑	1,072↑↑
Ser, ν(CO), δ(CO_2H)	967	966/957↑↑	967/957↑↑	967/956↑↑	965/955↑↑	966/956↑↑	965/955↑↑	965/955↑↑	965/955↑↑	965/955↑↑

[1]sym. = symmetric; asym. and as. = asymmetric; str. = stretching vibrations; def. = deformation vibrations; ↑ indicates small changes (relative to amide I band) in band intensities; ↑↑ indicates significant changes (relative to amide I band) in band intensities.

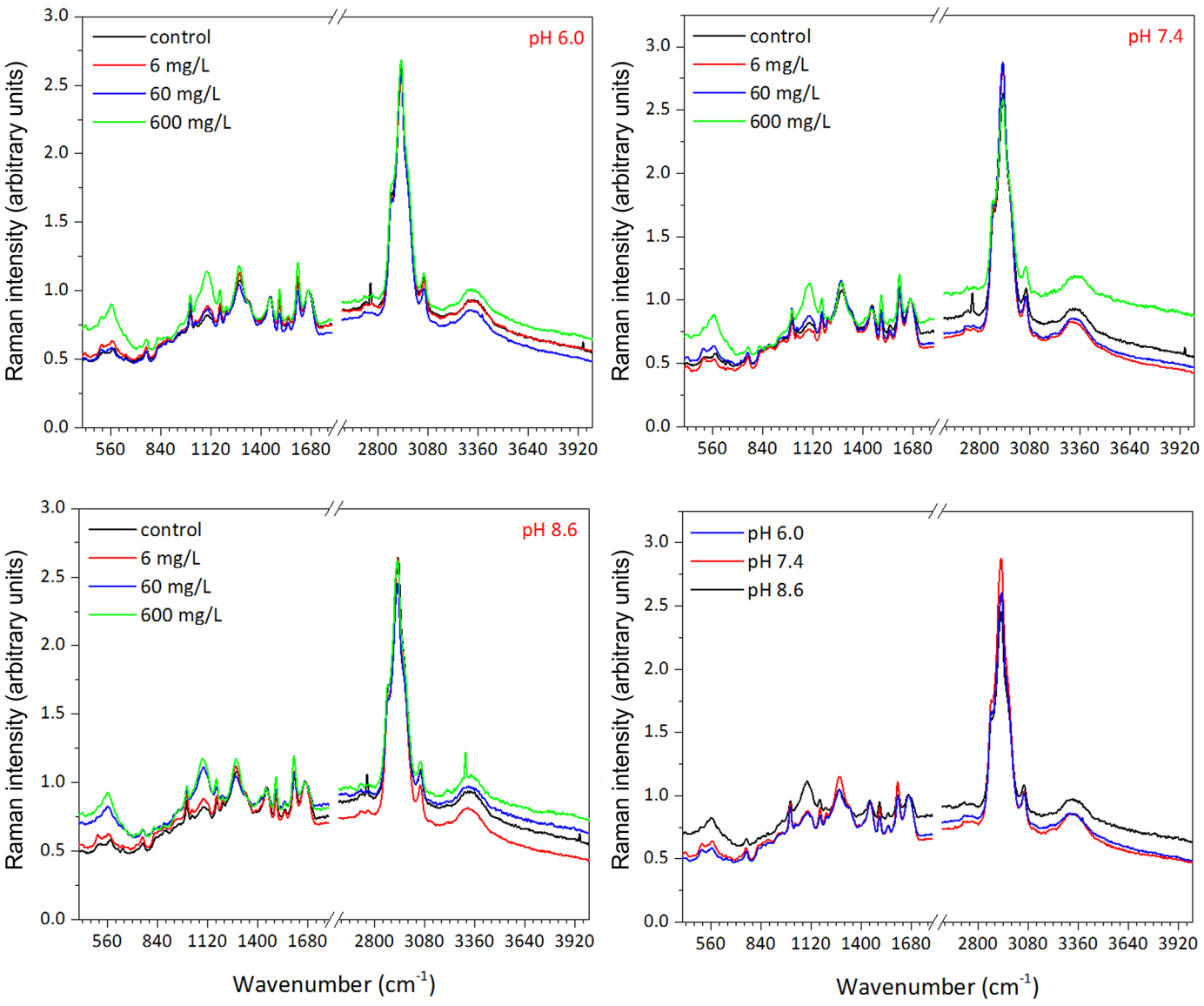

Figure 5. Raman spectra of native bovine lactoferrin (bLTF) and bLTF after interactions with Zn^{2+}.

600 cm^{-1} could arise due to the S–S stretching vibrations (Wen, 2007), whereas 417 cm^{-1} can be assigned to the Fe–O or Fe–NO complexes in iron-binding proteins (Ashton et al., 2017). The changes in intensities of some of the bands that correspond to S–S stretching vibration indicate the changes in the protein secondary and tertiary structure. Detailed changes in the bands and their intensities after the Zn-LTF interactions can be found in Table 2, where an increase or decrease in intensity was assigned by arrows.

Table 3 presents the results of ICP-MS determination of the 6 most common for proteins metal ions. According to obtained results, it is visible that Zn^{2+} binding occurred only at pH 7.4 and 8.6, but not at pH 6.0. The changes in the FTIR and Raman spectra observed for samples obtained at pH 6.0 may be due to the decrease of all metal contents in the sample as a result of the washing steps after the synthesis. Further discussion of the observed phenomena will be provided in the next section, which presents the proposed mechanisms of the metal-protein interaction.

Scanning electron microscopy images revealed minor changes in the protein surface structure. However, reasonable conclusions could not be derived because the main drawback of the method is a spatial resolution, which limits detailed characterization of the changes in protein structure after the interaction. In addition, observation of the protein structure is one

Table 2. The assigned bands derived from Raman spectra of native bovine lactoferrin (bLTF) and after interaction with Zn^{2+}[1]

Assignment	Native bLTF	Products of Zn-bLTF interaction								
		pH 6.0			pH 7.4			pH 8.6		
		6 mg/L	60 mg/L	600 mg/L	6 mg/L	60 mg/L	600 mg/L	6 mg/L	60 mg/L	600 mg/L
Hydrogen bonded O–H/N–H	3,335	3,342	3,315	3,335	3,315	3,312	3,312	3,323	3,327	3,308
N–H stretching vibration	3,060	3,057	3,057	3,060	3,058	3,057	3,058	3,057	3,058	3,057
Aliphatic and aromatic C–H sym/asym. str.	2,931	2,931	2,930	2,931	2,930	2,930	2,931	2,930	2,930	2,929
	2,878	2,876	2,875	2,879	2,876	2,875	2,876	2,876	2,875	2,874
	2,760	2,769	2,769	—	2,767	2,767	—	2,764	—	—
	2,736	2,735	2,724	—	2,726	2,726	—	2,724	—	—
Amide I	1,664	1,665	1,665	1,662	1,664	1,663	1,662	1,661	1,661	1,662
Tyr, Trp, Phe (ring modes)	1,604	1,603	1,602↑	1,603↑	1,603	1,602↑	1,602↑	1,602	1,602	1,601↑
Trp (indol ring)	1,550	1,552	1,550↓	1,551↓	1,551↓	1,549↓	1,556/1,548↑	1,549	1,549	1,549↑
Amide II	1,503	1,502	1,501↓	1,502	1,502	1,501	1,501↑	1,501	1,501	1,500↑
C-H def.	1,451	1,450	1,448	1,448	1,448	1,445↓	1,443↓	1,446	1,447	1,442
Glu, Asp ν(CO)	—	—	—	—	—	—	1,414	—	1,414	1,417
Trp (C_a–H) def., amide III	1,329	—	—	1,326↓	—	—	1,329	1,331	1,329	1,342
Amide III	1,284	1,280↑	1,277↓	1,276↑	1,278↑	1,278↑	1,281↑	1,276	1,275	1,277↑
Tyr (α-helix)	1,206	1,207	1,205	1,206↑	1,205	1,204	1,203	1,204	1,200↑	1,203↑
Tyr (CH_3)	1,172	1,170	1,169	1,169↑	1,170	1,169	1,168↑	1,169	1,168↑	1,168↑
C-N	1,101	1,099↑	1,101↑	1,098↑↑	1,102↓	1,097↑	1,101↑↑	1,094↑	1,098↑↑	1,090↑↑
Phe	1,033	1,034	1,032	—	1,031↓	1,030↑	—	1,031	—	—
Phe	1,005/960	1,004↑	1,003↑	1,004↑	1,003	1,002	1,003	1,002	1,003	1,003
Tyr (H-bonding)	881	881	878	876	878	880	883↑	877	876	875↓
	836	831	835	823↑	832	827	820↑	827↑	826↑	820↑
Trp (indol ring)	758	758	757	762↑	757↓	756↑	758↑	756↑	758↑	755↑
S–S TGT conformer	576	567↑	566	564↑↑	569↓	568↑	569↑↑	567	561↑↑	561↑↑
S–S, GGG conformer	519	510↑	508	508↑	510	510	513	506↑	505	510
Fe–O, Fe–NO	414	416	415	420	417	418	420	411	415	420

[1]sym. = symmetric; asym. and as. = asymmetric; str. = stretching vibrations; def. = deformation vibrations; ↑ indicates small changes (relative to amide I band) in band intensities; ↑↑ indicates significant changes (relative to amide I band) in band intensities.

Table 3. Results (± SD) for the inductively coupled plasma MS measurements of the metals content in the native bovine lactoferrin (bLTF) and after interaction with the Zn^{2+} solution of 6, 60, and 600 mg/L at pH 6.0, 7.4, and 8.6

	Metal					
Sample	Zn, mg/g	Fe, mg/g	Mg, µg/g	Na, mg/g	K, mg/g	Ca, mg/g
Native bLTF	0.017 ± 0.003	1.45 ± 0.06	9.5 ± 2.3	0.96 ± 0.16	0.11 ± 0.02	<LOQ[1]
pH 6.0						
6 mg/L	0.007 ± 0.005	1.24 ± 0.19	20.9 ± 0.6	0.28 ± 0.05	0.08 ± 0.02	<LOQ
60 mg/L	0.036 ± 0.002	1.17 ± 0.02	7.0 ± 3.6	<LOQ	<LOQ	<LOQ
600 mg/L	0.034 ± 0.003	0.80 ± 0.14	18.1 ± 1.0	<LOQ	<LOQ	<LOQ
pH 7.4						
6 mg/L	0.037 ± 0.005	1.22 ± 0.05	6.1 ± 0.9	<LOQ	<LOQ	<LOQ
60 mg/L	0.621 ± 0.022	1.25 ± 0.04	7.2 ± 1.4	<LOQ	<LOQ	<LOQ
600 mg/L	12.392 ± 0.720	1.14 ± 0.08	6.0 ± 0.6	<LOQ	<LOQ	<LOQ
pH 8.6						
6 mg/L	0.056 ± 0.005	1.18 ± 0.07	5.6 ± 0.4	—	<LOQ	<LOQ
60 mg/L	1.687 ± 0.080	1.11 ± 0.05	5.9 ± 1.0	—	<LOQ	<LOQ
600 mg/L	16.885 ± 1.426	1.02 ± 0.01	5.3 ± 6.7	—	<LOQ	<LOQ

[1]Limit of quantification.

of the main challenges in protein science (i.e., due to its low stability under exposure to high energies). The previous study with ovalbumin revealed that the Zn^{2+} interaction with proteins can lead to the formation of ZnO nanoparticles (Buszewski et al., 2021). Hence, the transmission electron microscopy (**TEM**)-energy-dispersive X-ray spectrometry analysis of the samples was performed. It was possible to detect Zn only in the samples prepared with the utilization of Zn^{2+} solution of 600 mg/L at pH 7.4 and 8.6. However, the formation of ZnO nanoparticles was not observed even for these samples. Thus, it could be deduced the formation of homogeneous metal-protein complexes at pH 7.4 and 8.6 (Figure 6).

Mechanisms of Zn-bLTF Interactions

The ICP-MS analysis revealed that after bLTF interaction with Zn^{2+} the changes in the quantity of all 6 of the most common metals that usually accompany proteins have occurred. What is interesting is that among all metals the Fe^{3+} has the highest affinity to bLTF (Takayama, 2012), but after interaction with zinc solutions in all utilized conditions, the iron content has decreased. The most dramatic decrease (i.e., ≈45%) was observed when Zn^{2+} solution with the concentration of 600 mg/L at pH 6.0 was used. The effect may be connected with 2 factors, and the first one is the acidic conditions that weaken the bond between Fe^{3+} and bLTF. The second factor is the competition of Zn^{2+} for metal-binding sites, which become more evident with a higher concentration of metal in the solution (Gurd and Wilcox, 1956). In all other cases, the decrease of iron content was in the range from 13 to 30 %. For pH 7.4 and 8.6, the main factor that should affect iron content is the presence of citrate ions in the solution. Citrate ions compete with bLTF for the metal ion. Generally, the native bLTF had 1.45 ± 0.06 mg/g of iron, which equals the ratio of metal:protein = 2.1:1, and thus means that both metal-binding sites were filled with iron. After the reaction, the portion of the iron was released from the protein, which enables the embedding of the Zn^{2+} into bLTF. However, at pH 6.0 the utilization of zinc solution of 6 mg/L also decreased the Zn^{2+} content. When solutions of 60 and 600 mg/L were used, a slight increase in Zn^{2+} content was observed. However, such small changes can be neglected because even they cannot compensate for the amount of vanished Fe^{3+}, leaving the bLTF unsaturated. Almost the same was the case when a solution of 6 mg/L at pH 7.4 and 8.6 was used. In turn, with the usage of zinc solution of 60 mg/L for both 7.4 and 8.6 the amount of bonded Zn^{2+} was already higher than vanished Fe^{3+}. Thus, it can be suggested that some portion of Zn^{2+} was bonded to surface functional groups of bLTF. The usage of the solution with a zinc concentration of 600 mg/L enables to bond ≈16 and 22 of Zn^{2+} at pH 7.4 and 8.6, respectively, which implies the formation of new metal-binding sites on the protein surface.

The deep chemistry of reactants should be considered for the proper description of the processes on the surface of the protein. Consideration of the participation of AA and peptides as building blocks of the protein can simplify the description. Subsequently, the extrapolation of obtained data for peptides and AA can be used for the description of interactions of more sophisticated molecules such as proteins. Such an approach was used by Sych et al. (2018) for the prediction of place(s) of formation of Ag clusters in protein. Tang and Skibsted (2016) reported the discussion of the bioavailability of

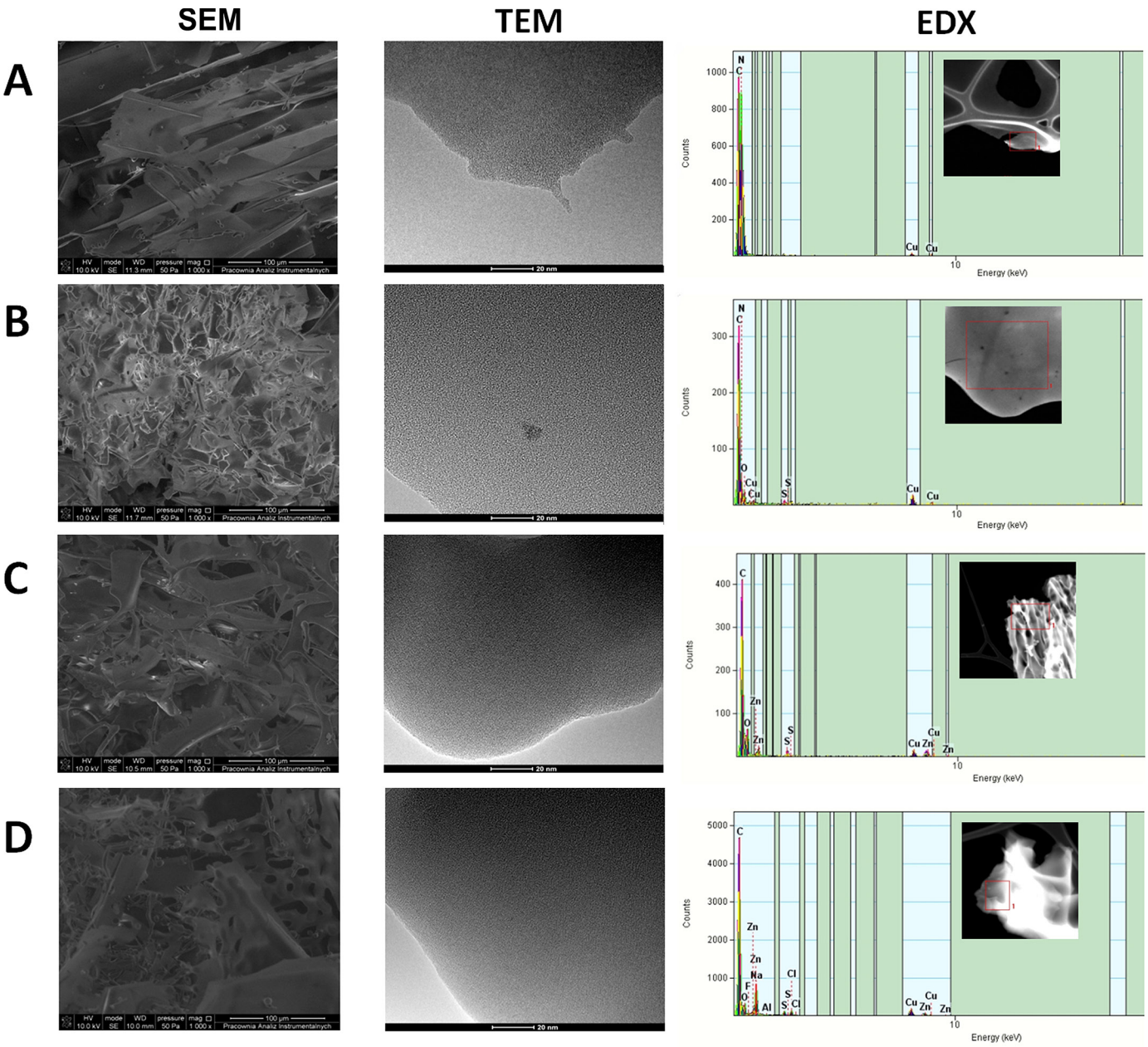

Figure 6. Results of scanning electron microscopy (SEM) and transmission electron microscopy (TEM)-energy-dispersive X-ray spectrometry (EDX) analysis of (A) native bovine lactoferrin (bLTF) and samples obtained with the utilization of Zn^{2+} solution of 600 mg/L at pH (B) 6.0, (C) 7.4, and (D) 8.6.

Zn^{2+} from whey. On the other hand, the authors reported the obtained data in an attempt to explain the role of individual AA in Zn^{2+} binding to the protein and therefore in Zn^{2+} homeostasis. Generally, this approach is well known from the first research on formation of metal ammine complexes (Gurd and Wilcox, 1956). However, such an approach should be applied carefully with consideration of the whole spectrum of intra- and supramolecular effects that can affect the interactions between the species. For instance, although Zn^{2+} ions form relatively stable complexes with glycine, this interaction is not significant for the binding of metal ions to protein. In this case, side chains of AA comprising the protein are of higher importance. However, for small peptides, it was shown that nitrogen from peptide bonds participates in metal complexation (Gurd and Wilcox, 1956). Thus, such molecules as glycine may also participate in the metal complexation.

Sulfhydryl (thiol) groups of side chains of the AA comprising the protein can form the strongest bonds with metals, particularly Zn^{2+} (Gurd and Wilcox, 1956; Tang and Skibsted, 2016). Cysteine is of high importance in proteins containing zinc finger structures, where metal-binding sites comprise different combinations of histidine and cysteine residues (Bou-Abdallah and Giffune, 2016). Bovine lactoferrin has 34 cysteines in its structure, which provides the respective amount of thiol groups (Pomastowski et al., 2016). However, free thiol groups are very reactive and undergo oxidation reaction with the formation of sulfenic (R-S–OH), sulfinic (R–SO_2H), and sulfonic (R–SO_3H) derivatives as well as the disulfide bond. In general, the presence of free thiol groups is distinctive for proteins located in the cytoplasm, whereas proteins in other compartments comprise oxidized thiol groups predominantly in form of disulfide bridges (Trivedi et al., 2009). In the bLTF, not only the number but also the position of cysteines predict 17 disulfide bonds (Schanbacher et al., 1993). The disulfide bridges are essential elements of the protein tertiary structure and are responsible for protein thermal stability (Trivedi et al., 2009). It was shown that Ag^+ and Hg^+ can easily break the disulfide bridges and form a highly stable bond with the thiol group (Gurd and Wilcox, 1956). For instance, Pomastowski et al. (2016) worked with both the experimental data as well as molecular dynamic analysis that have shown the involvement of disulfide bonds in Ag^+ binding to bLTF. However, a vast number of other metals are supposed to react with cystine (oxidized form of cysteine, containing disulfide bond) in a way similar to simple AA (Gurd and Wilcox, 1956). Still, the disulfide bond can undergo degradation in a basic environment by direct attack of hydroxyl anion on the sulfur atom with the formation of sulfenic acid and thiolate anion (Trivedi et al., 2009). Thus, although Zn^{2+} has a strong binding affinity to disulfides and cystine was thought to participate in intracellular Zn^{2+} homeostasis (Tang and Skibsted, 2016), the Zn^{2+} interactions with protein disulfide bonds are highly dependent on the reaction environment (Gurd and Wilcox, 1956). In our investigation, according to the Raman spectra, it can be observed that the changes in the signals corresponding to the disulfide bonds have occurred. The obtained data indicate the changes in the bLTF molecule conformation: the increase of signal near 560 cm^{-1} with an increase of Zn^{2+} in the complexes may indicate the prevalence of less stable TGT conformer of S-S bond in the molecule, whereas the signal near 510 cm^{-1} from more stable GGG conformer disappears (Wen, 2007). Such changes may not be connected to metal binding through a disulfide bond, but show the effect of Zn^{2+} on bLTF structure.

Numerous studies, including the one carried out by Buszewski et al., indicated that glutamic and aspartic acids play an important role in Zn^{2+} coordination by proteins (Jabeen et al., 2005; Pomastowski et al., 2014; Buszewski et al., 2020). Moreover, Zn^{2+} appears in water in form of aqua complex, which is considered as acid according to Brønsted-Lowry theory. The central ion in the complex causes the polarization of water molecules, resulting in a more labile proton. The dissociation of the proton leads to the formation of the aqua-hydroxo complex (Krężel and Maret, 2016). Similarly, the labile proton can interact with carboxylic groups of AA, leading to the formation of the hydroxo complex with subsequent transformation to ZnO, which can lead to the formation of ZnO-protein nanocomposites (Shi et al., 2008; Buszewski et al., 2021). The TEM analysis of synthesized Zn-bLTF complexes showed that zinc oxide nanoparticles did not form at any of the utilized conditions. Regarding the interactions between $Zn^{2+}$and carboxylic groups, it should be noted that they have an electrostatic character. In addition, it was shown that glutamic and aspartic acids have low zinc binding affinity, which implies the involvement of other nitrogen-containing residues to form stable complexes (Gurd and Wilcox, 1956; Yamauchi et al., 2002; Tang and Skibsted, 2016). The Lewis acid-base theory also indicates that because the Zn^{2+} belongs to borderline metal ions it has the highest affinity to ligands with nitrogen atoms such as nitrogen of peptide bond, imidazole ring, and guanidine (Alhazmi, 2019). In the present study, according to the results of ICP-MS measurements (Table 3), the binding of Zn^{2+} was not observed at pH 6.0. The effect can be explained by the chemistry of the bLTF. Apart from cysteine, histidine can bind metal most strongly. However, the imidazole group of free histidine has pK_a ≈5.99 (Belitz et al., 2009), whereas the inclusion of histidine to the protein chain shift the pK_a to higher values (Gurd and Wilcox, 1956), which implies that at pH 6.0 the availability of imidazole group for Zn^{2+} is limited. Thus, the binding of Zn^{2+} to imidazole groups may not appear. Instead, the interactions with carboxylic groups are weak, so it cannot hold the Zn^{2+} on the protein surface. By changing the pH to the higher values (7.4 and 8.6), the imidazole groups become more available, resulting in Zn^{2+} binding to protein. The evidence of Zn^{2+} interaction through carboxylic and imidazole groups can be observed from Raman and FTIR spectra from the changes in vibration intensity and shifts of appropriate bands, which appear in complexes synthesized in pH 7.4 and 8.6. Still, bLTF has only 9 histidines in its structure and 2 of them are the part of clefts in metal-binding sites. According to obtained results, both binding sites are filled with Fe ions (the bLTF:Fe^{3+} molar

ratio is nearly 1:2). Thus, the effect of histidine on the Zn^{2+} binding ability of bLTF is not dominant, whereas other nitrogen-containing functional groups have much higher pK_a, which indicates that a much more complex mechanism is involved in the process. Additionally, the FTIR spectra have revealed that serine and threonine may also be involved in the coordination of Zn^{2+}. Instead, the changes in the signals of aromatic AA, which are sensitive to cation-π interactions, may indicate the changes in the cation content in the complexes.

However, it should be noted that in the previous study on β-lactoglobulin interaction with zinc, the Zn^{2+} binding to protein was studied at pH 4.6, which is much lower than the pK_a of imidazole groups (Buszewski et al., 2020). The majority of publications indicate the pI for β-LG at pH 5.1 to 5.3 (e.g., by free-flow electrophoresis; Łapińska et al., 2017), but determined within the study of its interaction with Zn^{2+} was at pH 4.6 (by ζ-potential measurements; Buszewski et al., 2020). Thus, it may indicate the significant effect of the net charge of the protein on the effectiveness of the metal binding to protein. Bovine lactoferrin is a protein with high content of cationic residues. The presence of positively charged functional groups in AA has been shown to decrease the metal-binding constant, which was assumed due to electrostatic repulsion (Gurd and Wilcox, 1956). Similarly, the electrostatic repulsion may decrease Zn^{2+} binding ability to protein. Thus, in discussion of the protein as a charged macromolecule, it is reasonable to consider the pH value of the system as compared with pI. The pI value for bLTF in the present study was defined at pH ≈ 7.4 ± 0.2. However, the accuracy of this method still may not exclude the presence of the slight positive charge on the protein surface at this pH value, especially after binding of a small portion of Zn^{2+}. In addition, it implies that at pH 8.6 the charge of the protein is negative, whereas at pH 6.0 it is positive.

The effect of the protein charge can be observed on differences in metal binding in the solution at different pH. As it can be seen, the Zn^{2+} content in complexes obtained in pH 8.6 is 3 and 1.5 times higher than for pH 7.4 for the systems containing 60 and 600 mg/L of Zn^{2+}. Moreover, it is important to notice that the effect of concentration on the metal-protein binding can be observed. The results of measurements of metal adsorption on the protein from solution with 60 and 600 mg/L of Zn^{2+} and pH 8.6 was determined as 6.16 ± 0.28 and 64.60 ± 2.25 mg/g, respectively, whereas the Zn^{2+} content in the corresponding complexes was 1.69 ± 0.08 and 16.88 ± 1.42 mg/g, respectively. The protein can be considered a biocolloid, which according to the DLVO (Derjaguin–Landau–Verwey–Overbeek) theory implies the presence of a double electric layer and solvation shell on the surface of protein particles. Thus, the high metal concentration in the solution by affecting the solvation shell probably makes it possible for Zn^{2+} ions to interact with several functional groups, resulting in much higher stability of the complex. Therefore, the amount of Zn^{2+} that remains bounded to the protein after washing steps is higher. The effect also can be seen for Zn^{2+} adsorption from solutions at pH 7.4, but with less difference with the corresponding Zn^{2+} content in the complex. The adsorption was determined as 2.8 ± 0.22 and 19.0 ± 1.24 mg/g, whereas metal content in the corresponding complexes was 0.62 ± 0.2 and 12.39 ± 0.72 mg/g for 60 and 600 mg/L of Zn^{2+} concentration, respectively. However, while considering the interactions between Zn^{2+} and bLTF at pH 7.4 and 8.6, the presence of citrate and bicarbonate ions also should not be avoided. The Zn^{2+} binding constants to bicarbonate and citrate indicate that in both systems Zn^{2+} ions appear predominantly in the form of citrate complex (Fouillac and Criaud, 1984; Krężel and Maret, 2016), which implies the competition of citrate anion with protein for Zn^{2+}. Thus, the higher adsorption of Zn^{2+} in the system with higher metal concentration may not indicate the changes in the shielding effect of the double electric layer, but the higher availability of metal ions, as the concentration of citrate remains stable. Still, the buffer with pH 8.6 comprises a higher concentration of citrate anion and the binding capability of protein in pH 8.6 is higher, which may indicate the higher influence of protein net charge on its metal-binding efficiency.

However, the tertiary structure of the protein also affects the metal-binding properties. The formation of stable metal-protein complexes involves the coordination of several functional groups by a metal ion. Thus, an appropriate number of functional groups is not sufficient because their location is also important. Additionally, this may affect the thermodynamics of the process (Gurd and Wilcox, 1956). It is well known that the changes in free Gibbs energy must have a negative value for the occurrence of spontaneous reaction. The chelation of Zn^{2+} ions by proteins implies an enthalpy effect, which according to Tang and Skibsted (2016) for bLTF was determined as $\Delta H = -100$ kJ/mol. However, the entropy for the reaction was determined as $\Delta S = -250.5$ J/mol K (measured in pH 7.4). The Zn^{2+} chelation by bLTF implies the release of water molecules from the aqua complex, which leads to the increase in entropy of the system. The determined negative value of the entropy may indicate the changes in the flexibility of the protein molecule. It is even more interesting to investigate how the pH difference may affect the

thermodynamics of the process, which is the aim of our future study. The pH and ionic strength of the system affect the conformation of the protein molecule and therefore the bLTF metal-binding properties as well as the thermodynamics of the process (Gurd and Wilcox, 1956).

CONCLUSIONS

This study presents the results for the bLTF interaction with Zn^{2+} at 3 different pH and 3 different metal concentrations. Study revealed that the Zn^{2+} immobilization onto protein has occurred in the solution at pH 7.4 and 8.6, but not at pH 6.0. Obtained data indicate that the availability of nitrogen-containing functional groups and protein net charge (which can be manipulated by pH changes) have a significant impact on the ability of protein to bind Zn^{2+}. Moreover, the higher ionic strength of the solution, in particular the Zn^{2+} concentration, increases the probability of metal ion chelation through several functional groups of the protein and thus formation of stable metallocomplexes. Finally, the pH and the ionic strength should affect the conformation of the protein, which also may result in the formation of structures favorable for Zn^{2+} binding. However, it is noteworthy to mention that changes in protein tertiary structure also change the thermodynamics of the process.

ACKNOWLEDGMENTS

This work was financially supported in the framework of the project "Advanced Biocomposites for Tomorrow's Economy BIOG-NET" (FNP POIR.04.04.00-00-1792/18-00), which is carried out within the TEAM-NET programme of the Foundation for Polish Science (Warsaw) co-financed by the European Union under the European Regional Development Fund. Oleksandra Pryshchepa, Paweł Pomastowski, and Bogusław Buszewski are members of Toruń Center of Excellence "Towards Personalized Medicine" (Toruń, Poland) operating under Excellence Initiative-Research University. In addition, the authors acknowledge Katarzyna Rafińska for help with TEM and ATR-FTIR analysis as well as Adrian Gołębiowski for ICP-MS measurements. The authors have not stated any conflicts of interest.

REFERENCES

Ainscough, E. W., A. M. Brodie, and J. E. Plowman. 1980. Zinc transport by lactoferrin in human milk. Am. J. Clin. Nutr. 33:1314–1315. https://doi.org/10.1093/ajcn/33.6.1314.

Alhazmi, H. 2019. FT-IR spectroscopy for the identification of binding sites and measurements of the binding interactions of important metal ions with bovine serum albumin. Sci. Pharm. 87:5. https://doi.org/10.3390/scipharm87010005.

Andersson, Y., S. Lindquist, C. Lagerqvist, and O. Hernell. 2000. Lactoferrin is responsible for the fungistatic effect of human milk. Early Hum. Dev. 59:95–105. https://doi.org/10.1016/S0378-3782(00)00086-4.

Ashton, L., V. L. Brewster, E. Correa, and R. Goodacre. 2017. Detection of glycosylation and iron-binding protein modifications using Raman spectroscopy. Analyst (Lond.) 142:808–814. https://doi.org/10.1039/C6AN02516A.

Auld, D. S. 2013. Zinc-Binding Sites in Proteins. Springer.

Baker, E. N. 1994. Structure and reactivity of transferrins. Adv. Inorg. Chem. 41:389–469. https://doi.org/10.1016/S0898-8838(08)60176-2.

Barth, A. 2007. Infrared spectroscopy of proteins. Biochim. Biophys. Acta 1767:1073–1101. https://doi.org/10.1016/j.bbabio.2007.06.004.

Belitz, H. D., W. Grosch, and P. Schieberle. 2009. Food Chemistry. Springer.

Bong, C. W., F. M. Alfatti, F. A. Zam, Y. Obayashi, and S. Suzuki. 2010. The effect of zinc exposure on the bacteria abundance and proteolytic activity in seawater. Pages 57–63 in 57 Interdisciplinary Studies on Environmental Chemistry—Biological Responses to Contaminants. Terrapub.

Bou-Abdallah, F., and T. R. Giffune. 2016. The thermodynamics of protein interactions with essential first row transition metals. Biochim. Biophys. Acta 1860:879–891. https://doi.org/10.1016/j.bbagen.2015.11.005.

Buszewski, B., A. Rodzik, V. Railean-Plugaru, M. Sprynskyy, and P. Pomastowski. 2020. A study of zinc ions immobilization by β-lactoglobulin. Colloids Surf. A Physicochem. Eng. Asp. 591:124443. https://doi.org/10.1016/j.colsurfa.2020.124443.

Buszewski, B., P. Žuvela, A. Król-Górniak, V. Railean-Plugaru, A. Rogowska, M. W. Wong, M. Yi, A. Rodzik, M. Sprynskyy, and P. Pomastowski. 2021. Interactions of zinc aqua complexes with ovalbumin at the forefront of the Zn2+/ZnO-OVO hybrid complex formation mechanism. Appl. Surf. Sci. 542:148641. https://doi.org/10.1016/j.apsusc.2020.148641.

Corsetti, S., T. Rabl, D. McGloin, and J. Kiefer. 2017. Intermediate phases during solid to liquid transitions in long-chain n-alkanes. Phys. Chem. Chem. Phys. 19:13941–13950. https://doi.org/10.1039/C7CP01468F.

Du, Q.-Y., D.-Q. Lin, Z.-S. Xiong, and S.-J. Yao. 2013. One-step purification of lactoferrin from crude sweet whey using cation-exchange expanded bed adsorption. Ind. Eng. Chem. Res. 52:2693–2699. https://doi.org/10.1021/ie302606z.

Dullius, A., M. I. Goettert, and C. F. V. de Souza. 2018. Whey protein hydrolysates as a source of bioactive peptides for functional foods – Biotechnological facilitation of industrial scale-up. J. Funct. Foods 42:58–74. https://doi.org/10.1016/j.jff.2017.12.063.

Fischer, R., H. Debbabi, A. Blais, M. Dubarry, M. Rautureau, P. N. Boyaka, and D. Tome. 2007. Uptake of ingested bovine lactoferrin and its accumulation in adult mouse tissues. Int. Immunopharmacol. 7:1387–1393. https://doi.org/10.1016/j.intimp.2007.05.019.

Fouillac, C., and A. Criaud. 1984. Carbonate and bicarbonate trace metal complexes: Critical reevaluation of stability constants. Geochem. J. 18:297–303. https://doi.org/10.2343/geochemj.18.297.

Franco, I., M. D. Pérez, C. Conesa, M. Calvo, and L. Sánchez. 2018. Effect of technological treatments on bovine lactoferrin: An overview. Food Res. Int. 106:173–182. https://doi.org/10.1016/j.foodres.2017.12.016.

Gołębiowski, A., P. Pomastowski, A. Rodzik, A. Król-Górniak, T. Kowalkowski, M. Górecki, and B. Buszewski. 2020. Isolation and self-association studies of beta-lactoglobulin. Int. J. Mol. Sci. 21:9711. https://doi.org/10.3390/ijms21249711.

Grigorieva, D. V., I. V. Gorudko, E. V. Shamova, M. S. Terekhova, E. V. Maliushkova, I. V. Semak, S. N. Cherenkevich, A. V. Sokolov, and A. V. Timoshenko. 2019. Effects of recombinant human lactoferrin on calcium signaling and functional responses of human

neutrophils. Arch. Biochem. Biophys. 675:108122. https://doi.org/10.1016/j.abb.2019.108122.
Gurd, F. R. N., and P. E. Wilcox. 1956. Complex formation between metallic cations and proteins, peptides, and amino acids. Adv. Protein Chem. 11:311–427. https://doi.org/10.1016/s0065-3233(08)60424-6.
Ianni, A., M. Iannaccone, C. Martino, D. Innosa, L. Grotta, F. Bennato, and G. Martino. 2019. Zinc supplementation of dairy cows: Effects on chemical composition, nutritional quality and volatile profile of Giuncata cheese. Int. Dairy J. 94:65–71. https://doi.org/10.1016/j.idairyj.2019.02.014.
Jabeen, T., S. Sharma, N. Singh, A. Bhushan, and T. P. Singh. 2005. Structure of the zinc-saturated C-terminal lobe of bovine lactoferrin at 2.0 Å resolution. Acta Crystallogr. D Biol. Crystallogr. 61:1107–1115. https://doi.org/10.1107/S0907444905016069.
Jacob, C. R., S. Luber, and M. Reiher. 2009. Analysis of secondary structure effects on the IR and Raman spectra of polypeptides in terms of localized vibrations. J. Phys. Chem. B 113:6558–6573. https://doi.org/10.1021/jp900354g.
Kambe, T., T. Tsuji, A. Hashimoto, and N. Itsumura. 2015. The physiological, biochemical, and molecular roles of zinc transporters in zinc homeostasis and metabolism. Physiol. Rev. 95:749–784. https://doi.org/10.1152/physrev.00035.2014.
Kawakami, H., S. Dosako, and I. Nakajima. 1993. Effect of lactoferrin on iron solubility under neutral conditions. Biosci. Biotechnol. Biochem. 57:1376–1377. https://doi.org/10.1271/bbb.57.1376.
Kotting, C., and K. Gerwert. 2007. Protein reactions: Resolved with tr-FT-IR. Spectrosc. Eur. 19:19–23.
Krężel, A., and W. Maret. 2016. The biological inorganic chemistry of zinc ions. Arch. Biochem. Biophys. 611:3–19. https://doi.org/10.1016/j.abb.2016.04.010.
Lambert, L. A. 2012. Molecular evolution of the transferrin family and associated receptors. Biochim. Biophys. Acta 1820:244–255. https://doi.org/10.1016/j.bbagen.2011.06.002.
Łapińska, U., K. L. Saar, E. V. Yates, T. W. Herling, T. Müller, P. K. Challa, C. M. Dobson, and T. P. J. Knowles. 2017. Gradient-free determination of isoelectric points of proteins on chip. Phys. Chem. Chem. Phys. 19:23060–23067. https://doi.org/10.1039/C7CP01503H.
McDevitt, C. A., A. D. Ogunniyi, E. Valkov, M. C. Lawrence, B. Kobe, A. G. McEwan, and J. C. Paton. 2011. A Molecular Mechanism for Bacterial Susceptibility to Zinc. PLoS Pathog. 7:e1002357. https://doi.org/10.1371/journal.ppat.1002357.
Mizutani, K., M. Toyoda, and B. Mikami. 2012. X-ray structures of transferrins and related proteins. Biochim. Biophys. Acta 1820:203–211. https://doi.org/10.1016/j.bbagen.2011.08.003.
Nandiyanto, A. B. D., R. Oktiani, and R. Ragadhita. 2019. How to read and interpret FTIR spectroscope of organic material. Indones. J. Sci. Technol. 4:97. https://doi.org/10.17509/ijost.v4i1.15806.
Oćwieja, M., Z. Adamczyk, M. Morga, and K. Kubiak. 2015. Silver particle monolayers — Formation, stability, applications. Adv. Colloid Interface Sci. 222:530–563. https://doi.org/10.1016/j.cis.2014.07.001.
Ortiz, Y., E. García-Amézquita, C. H. Acosta, and D. R. Sepúlveda. 2017. Functional Dairy Products. Pages 67–103 in Global Food Security and Wellness. G. V. Barbosa-Cánovas, G. M. Pastore, K. Candoğan, I. G. M. Meza, S. Caetano da Silva Lannes, K. Buckle, R. Y. Yada, and A. Rosenthal, ed. Springer.
Pomastowski, P., M. Sprynskyy, and B. Buszewski. 2014. The study of zinc ions binding to casein. Colloids Surf. B Biointerfaces 120:21–27. https://doi.org/10.1016/j.colsurfb.2014.03.009.
Pomastowski, P., M. Sprynskyy, P. Žuvela, K. Rafińska, M. Milanowski, J. J. Liu, M. Yi, and B. Buszewski. 2016. Silver-lactoferrin nanocomplexes as a potent antimicrobial agent. J. Am. Chem. Soc. 138:7899–7909. https://doi.org/10.1021/jacs.6b02699.
Roosen-Runge, F., B. S. Heck, F. Zhang, O. Kohlbacher, and F. Schreiber. 2013. Interplay of pH and binding of multivalent metal ions: Charge inversion and reentrant condensation in protein solutions. J. Phys. Chem. B 117:5777–5787. https://doi.org/10.1021/jp401874t.
Rygula, A., K. Majzner, K. M. Marzec, A. Kaczor, M. Pilarczyk, and M. Baranska. 2013. Raman spectroscopy of proteins: A review. J. Raman Spectrosc. 44:1061–1076. https://doi.org/10.1002/jrs.4335.
Sabra, S., and M. M. Agwa. 2020. Lactoferrin, a unique molecule with diverse therapeutical and nanotechnological applications. Int. J. Biol. Macromol. 164:1046–1060. https://doi.org/10.1016/j.ijbiomac.2020.07.167.
Salgın, S., U. Salgın, and S. Bahadır. 2012. Zeta potentials and isoelectric points of biomolecules: The effects of ion types and ionic strengths. Int. J. Electrochem. Sci. 7:12404–12414.
Santos, H. O., F. J. Teixeira, and B. J. Schoenfeld. 2020. Dietary vs. pharmacological doses of zinc: A clinical review. Clin. Nutr. 39:1345–1353. https://doi.org/10.1016/j.clnu.2019.06.024.
Schanbacher, F. L., R. E. Goodman, and R. S. Talhouk. 1993. Bovine mammary lactoferrin: Implications from messenger ribonucleic acid (mRNA) sequence and regulation contrary to other milk proteins. J. Dairy Sci. 76:3812–3831. https://doi.org/10.3168/jds.S0022-0302(93)77725-5.
See, Y. P., P. M. Olley, and G. Jackowski. 1985. The effects of high salt concentrations in the samples on molecular weight determination in sodium dodecyl sulfate polyacrylamide gel electrophoresis. Electrophoresis 6:382–387. https://doi.org/10.1002/elps.1150060806.
Shevchenko, A., H. Tomas, J. Havli, J. V. Olsen, and M. Mann. 2006. In-gel digestion for mass spectrometric characterization of proteins and proteomes. Nat. Protoc. 1:2856–2860. https://doi.org/10.1038/nprot.2006.468.
Shi, L., J. Zhou, and S. Gunasekaran. 2008. Low temperature fabrication of ZnO–whey protein isolate nanocomposite. Mater. Lett. 62:4383–4385. https://doi.org/10.1016/j.matlet.2008.07.038.
Shilpashree, B. G., S. Arora, S. Kapila, and V. Sharma. 2020. Whey protein-iron or zinc complexation decreases pro-oxidant activity of iron and increases iron and zinc bioavailability. Lebensm. Wiss. Technol. 126:109287. https://doi.org/10.1016/j.lwt.2020.109287.
Simpson, R. J. 2010. Stabilization of Proteins for Storage. Cold Spring Harbor Protocols. https://doi.org/10.1101/pdb.top79.
Singh, B. R., D. B. DeOliveira, F.-N. Fu, and M. P. Fuller. 1993. Fourier transform infrared analysis of amide III bands of proteins for the secondary structure estimation. Pages 47–55 in Biomolecular Spectroscopy III. SPIE.
Socrates, G. G. 2004. Infrared and Raman Characteristic Group Frequencies: Tables and Charts. 3rd ed. John Wiley & Sons, Ltd.
Sych, T. S., A. A. Buglak, Z. V. Reveguk, V. A. Pomogaev, R. R. Ramazanov, and A. I. Kononov. 2018. Which amino acids are capable of nucleating fluorescent silver clusters in proteins? J. Phys. Chem. C 122:26275–26280. https://doi.org/10.1021/acs.jpcc.8b08979.
Takayama, Y. 2012. Lactoferrin and Its Role in Wound Healing. Springer.
Tang, N., and L. H. Skibsted. 2016. Zinc bioavailability from whey. Enthalpy-entropy compensation in protein binding. Food Res. Int. 89:749–755. https://doi.org/10.1016/j.foodres.2016.10.002.
Trivedi, M., J. Laurence, and T. Siahaan. 2009. The role of thiols and disulfides on protein stability. Curr. Protein Pept. Sci. 10:614–625. https://doi.org/10.2174/138920309789630534.
van Veen, H. A., M. E. J. Geerts, P. H. C. Van Berkel, and J. H. Nuijens. 2004. The role of N-linked glycosylation in the protection of human and bovine lactoferrin against tryptic proteolysis. Eur. J. Biochem. 271:678–684. https://doi.org/10.1111/j.1432-1033.2003.03965.x.
Voswinkel, L., T. Vogel, and U. Kulozik. 2016. Impact of the iron saturation of bovine lactoferrin on adsorption to a strong cation exchanger membrane. Int. Dairy J. 56:134–140. https://doi.org/10.1016/j.idairyj.2016.01.008.
Waarts, B.-L., O. J. C. Aneke, J. M. Smit, K. Kimata, R. Bittman, D. K. F. Meijer, and J. Wilschut. 2005. Antiviral activity of human lactoferrin: Inhibition of alphavirus interaction with heparan sulfate. Virology 333:284–292. https://doi.org/10.1016/j.virol.2005.01.010.
Wang, B. 2016. Molecular determinants of milk lactoferrin as a bioactive compound in early neurodevelopment and cognition. J. Pediatr. 173:S29–S36. https://doi.org/10.1016/j.jpeds.2016.02.073.

Wei, Z., T. Nishimura, and S. Yoshida. 2000. Presence of a glycan at a potential N-glycosylation site, Asn-281, of bovine lactoferrin. J. Dairy Sci. 83:683–689. https://doi.org/10.3168/jds.S0022-0302(00)74929-0.

Wen, Z. 2007. Raman spectroscopy of protein pharmaceuticals. J. Pharm. Sci. 96:2861–2878. https://doi.org/10.1002/jps.20895.

Yamauchi, O., A. Odani, and M. Takani. 2002. Metal–amino acid chemistry. Weak interactions and related functions of side chain groups. J. Chem. Soc. Dalt. Trans. 18:3411–3421. https://doi.org/10.1039/B202385G.

Ye, X., S. Yoshida, and T. B. Ng. 2000. Isolation of lactoperoxidase, lactoferrin, α-lactalbumin, β-lactoglobulin B and β-lactoglobulin A from bovine rennet whey using ion exchange chromatography. Int. J. Biochem. Cell Biol. 32:1143–1150. https://doi.org/10.1016/S1357-2725(00)00063-7.

Yoshida, S., Z. Wei, Y. Shinmura, and N. Fukunaga. 2000. Separation of lactoferrin-a and -b from bovine colostrum. J. Dairy Sci. 83:2211–2215. https://doi.org/10.3168/jds.S0022-0302(00)75104-6.

Yoshida, S., and Ye-Xiuyun.. 1991. Isolation of lactoperoxidase and lactoferrins from bovine milk acid whey by carboxymethyl cation exchange chromatography. J. Dairy Sci. 74:1439–1444. https://doi.org/10.3168/jds.S0022-0302(91)78301-X.

ORCIDS

Oleksandra Pryshchepa https://orcid.org/0000-0001-9586-7069
Gulyaim Sagandykova https://orcid.org/0000-0001-6778-4653
Joanna Rudnicka https://orcid.org/0000-0001-5550-4001
Paweł Pomastowski https://orcid.org/0000-0002-1594-0623
Bogusław Buszewski https://orcid.org/0000-0002-5482-7500